

2000

# H-1 Nuclear Magnetic Resonance Spin-Lattice Relaxation, C-13 Magic-Angle-Spinning Nuclear Magnetic Resonance Spectroscopy, Differential Scanning Calorimetry, and X-Ray Diffraction of Two Polymorphs of 2,6-Di-Tert-Butylnaphthalene

Peter A. Beckmann

*Bryn Mawr College*, pbeckman@brynmawr.edu

Kendra S. Burbank

Katharine M. Clemo

Erin N. Slonaker

Kristin Averill

*See next page for additional authors*

[Let us know how access to this document benefits you.](#)

Follow this and additional works at: [http://repository.brynmawr.edu/physics\\_pubs](http://repository.brynmawr.edu/physics_pubs)

 Part of the [Physics Commons](#)

---

## Custom Citation

P.A. Beckmann *et al.*, *J. Chem. Phys.* **113**, 1958 (2000).

This paper is posted at Scholarship, Research, and Creative Work at Bryn Mawr College. [http://repository.brynmawr.edu/physics\\_pubs/25](http://repository.brynmawr.edu/physics_pubs/25)

For more information, please contact [repository@brynmawr.edu](mailto:repository@brynmawr.edu).

---

**Authors**

Peter A. Beckmann, Kendra S. Burbank, Katharine M. Clemo, Erin N. Slonaker, Kristin Averill, Cecil Dybowski, Joshua S. Figueroa, Alicia Glatfelter, Stephanie Koch, Louise M. Liable-Sands, and Arnold L. Rheingold

# $^1\text{H}$ nuclear magnetic resonance spin-lattice relaxation, $^{13}\text{C}$ magic-angle-spinning nuclear magnetic resonance spectroscopy, differential scanning calorimetry, and x-ray diffraction of two polymorphs of 2,6-di-*tert*-butylnaphthalene

Peter A. Beckmann, Kendra S. Burbank, Katharine M. Clemo, and Erin N. Slonaker  
*Department of Physics, Bryn Mawr College, Bryn Mawr, Pennsylvania 19010-2899*

Kristin Averill, Cecil Dybowski, Joshua S. Figueroa, Alicia Glatfelter, Stephanie Koch, Louise M. Liable-Sands, and Arnold L. Rheingold  
*Department of Chemistry and Biochemistry, University of Delaware, Newark, Delaware 19716-2522*

(Received 22 March 2000; accepted 1 May 2000)

Polymorphism, the presence of structurally distinct solid phases of the same chemical species, affords a unique opportunity to evaluate the structural consequences of intermolecular forces. The study of two polymorphs of 2,6-di-*tert*-butylnaphthalene by single-crystal x-ray diffraction, differential scanning calorimetry (DSC),  $^{13}\text{C}$  magic-angle-spinning (MAS) nuclear magnetic resonance (NMR) spectroscopy, and  $^1\text{H}$  NMR spin-lattice relaxation provides a picture of the differences in structure and dynamics in these materials. The subtle differences in structure, observed with x-ray diffraction and chemical shifts, strikingly affect the dynamics, as reflected in the relaxation measurements. We analyze the dynamics in terms of both discrete sums and continuous distributions of Poisson processes. © 2000 American Institute of Physics.

[S0021-9606(00)50229-3]

## I. INTRODUCTION

The development of solid structure by nonpolar or weakly polar molecular solids is not a well-understood process. van der Waals forces between molecules are weak, and the free-energy differences among various multimolecule structures are rarely more than a few kcal/mol. As a consequence, one observes the formation of various solid structures, depending on the conditions of preparation of the solid. Despite the often-minor differences among these forms, many characteristics such as magnetic and optical properties, dissolution, and ultimately reactivity are determined by the solid's phase structure. Such differences in material properties abound in fields as diverse as high explosives, pharmaceutical chemistry, polymer chemistry, and metallurgy. On a fundamental level, understanding how molecular aggregation produces specific structures is a prerequisite to controlling the production of materials whose properties may be specified at the few-molecule level, such as in the creation of nanostructures.

2,6-di-*tert*-butylnaphthalene (2,6-DTN; Fig. 1) crystallizes in two polymorphic forms, designated **A** and **E**. The molecular structure is not significantly different in these two forms, and there are not significantly different intermolecular associations (e.g., hydrogen bonding) to distinguish the two polymorphs. The principal distinguishing factor between the two forms is the number of crystallographically independent molecules comprising the periodically repeating motif.

To understand the structure and dynamics in these two polymorphs, we have investigated them with x-ray diffraction,  $^{13}\text{C}$  magic-angle-spinning (MAS) NMR spectroscopy, differential scanning calorimetry (DSC), and measurements

of the temperature and frequency dependencies of the  $^1\text{H}$  NMR spin-lattice relaxation time,  $T_1$ .<sup>1</sup> One of the crystalline structures of the two polymorphs is complex and subtly different in ways that only a combination of analyses can fully elucidate. The results suggest that complementary analyses give a thorough picture of these kinds of materials at the "several-molecule" or mesoscopic scale.

## II. EXPERIMENTAL RESULTS

### A. Sample preparation

We examined 2,6-DTN which was either obtained commercially from K&K Industries or synthesized in our laboratory.<sup>2</sup> The quoted purity of the commercial sample before further purification was 98% and its quoted melting point was 421 K. All materials were sublimed or recrystallized before use. There were no discernible differences between samples made from the commercial material or synthesized in our laboratory.

In our examination of 2,6-DTN, we obtained solids by crystallization from 18 organic solvents. X-ray analyses showed that, from 17 of these, the less symmetric polymorph **E** was preferentially formed. **E** is monoclinic, and crystallizes in the noncentrosymmetric space group  $P2_1$  ( $Z=12$ ,  $Z'=6$ ), as discussed in greater detail below.

Crystallization from acetone at room temperature uniquely produces a metastable phase, designated polymorph **A**. It is *ca.* 4% denser than **E**, it is also monoclinic, and it crystallizes in the centrosymmetric space group  $P2_1/c$  ( $Z=2$  and  $Z'=1/2$ ), as discussed in greater detail below. Less symmetrical forms with more degrees of freedom may pre-

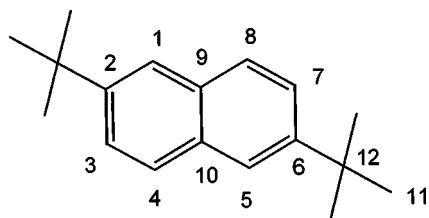


FIG. 1. 2,6-di-*tert*-butylnaphthalene (2,6-DTN). The numbering scheme for assignment of carbon NMR spectra is indicated.

vail at higher temperatures due to their higher vibrational entropies, but at lower temperatures denser packing arrangements with greater order commonly prevail. The more symmetrical and slightly denser **A** would, therefore, be expected to be the thermodynamically more stable form at 0 K. However, at 350 K, where vibrational entropy is a dominant factor, conversion of **A** to **E** is fairly rapid, placing an upper limit on the temperature at which **A** can be studied.

## B. Differential scanning calorimetry

Differential scanning calorimetry of **A** between 290 and 450 K using a Mettler TA 2000 DSC reveals a complex weakly endothermic transition beginning at 314 K and a second, much larger, simple endotherm at 421 K, the melting point. The 314 K event has some structure, suggesting that it is composed of both endo- and exothermic terms. We interpret this as the irreversible reorganization of the lattice from **A** to **E** occurring in nucleated stages, which below 314 K is inhibited by some thermal barrier to reorganization. Overall, the process is endothermic and clearly driven by a large entropy increase accompanying the **A**-to-**E** conversion.

At 353 K and 1 torr, 2,6-DTN sublimates to form large crystals of **E**. The size of the crystals may be taken as an indication that at this temperature **E** is obtained directly, in

accord with our observations that the solid–solid **A**-to-**E** conversion is crystal destructive leading to a powdering of the sample. In contrast to the behavior of **A**, differential scanning calorimetric measurements of **E** through the same temperature range showed only the endothermic event at 421 K and no **E**-to-**A** transition on cooling.

## C. X-ray crystallography

Data for both polymorphs were collected with a charge coupled device (CCD)-modified, four-circle P4 Siemens diffractometer. Crystallographic data for **E** were obtained from a specimen grown by sublimation. All computations used the SHELXTL program library (G. Sheldrick, Bruker AXS, Madison, WI). Crystallographic data are collected in Table I.

The space group,  $P2_1/c$ , for **A** is uniquely determined by the systematic absences in the diffraction data. **A** is satisfactorily refined with anisotropic thermal parameters for nonhydrogen atoms and with idealized hydrogen-atom contributions. The unit cell of **A** is shown in Fig. 2(a) and the molecular structure is shown in Fig. 3. The unit cell contains two complete molecules. The molecule rigorously possesses  $2/m(C_{2v})$  symmetry, with a twofold axis perpendicular to the aromatic plane at the midpoint of the C(5)–C(5a) vector (Fig. 3), coinciding with the molecular and crystallographic inversion center ( $Z' = 1/2$ ). Note that Fig. 3 shows the standard x-ray diffraction numbering scheme, whereas Fig. 1 shows the standard organic chemistry numbering scheme used in identifying the  $^{13}\text{C}$  NMR spectra. [The C(5) and C(5a) positions in Fig. 3 correspond to the C9 and C10 positions in Fig. 1.] In the lattice, the layers of molecules in **A** are arranged end to end with cleavage planes at the surfaces formed by the *tert*-butyl groups. Within the layers, the molecules are arranged edge to side such that the closest contacts (2.8–2.9 Å) are between hydrogen and carbon atoms. The angle between the aromatic planes of adjacent molecules is 66.5°.

The x-ray diffraction results for **E** are considerably more complex than for **A**. For **E**, either the space group  $P2_1$  or  $P2_1/m$  is indicated. The statistical distribution of normalized structure factors strongly favors the noncentrosymmetric alternative,  $P2_1$ , with 12 molecules per unit cell [ $Z = 12$ , Fig. 2(b)]. There are six crystallographically independent, commensurately modulated molecules ( $Z' = 6$ ) forming the asymmetric unit (Fig. 4). In the rejected centrosymmetric choice, each of the six independent molecules is highly disordered across a crystallographic mirror plane. In  $P2_1$ , no interatomic correlations greater than 0.5 are observed. Refinement proceeded less satisfactorily than for **A** due to the presence of a quasisuperlattice structure that caused the majority of the collected data to be extremely weak. In support of the superlattice description is the observation that reflections with  $h \neq 3n$  are about 20-fold weaker than reflections with  $h = 3n$ . This is consistent with the modulation vector being aligned along the  $a$  axis, as seen in Fig. 2(b). The hand of the lattice for **E** is arbitrary.

In **A** the molecules are arranged head to head, whereas in **E** they are arranged in interleaved layers in which the closest intermolecular contacts are formed by hydrogen atoms of the *tert*-butyl groups and aromatic carbon and hydro-

TABLE I. Crystallographic data for two polymorphs of 2,6-di-*tert*-butylnaphthalene.

Polymorph	<b>E</b>	<b>A</b>
Crystal growth	sublimation	from acetone
Formula	$\text{C}_{18}\text{H}_{24}$	$\text{C}_{18}\text{H}_{24}$
Formula weight	168.31	168.31
Color, crystal habit	colorless block	colorless plate
Crystal system	monoclinic	monoclinic
Space group	$P2_1$	$P2_1/c$
$a$ , Å	19.6636(1)	11.3649(4)
$b$ , Å	12.6712(3)	9.9406(3)
$c$ , Å	19.7853(3)	6.6728(2)
$\beta$ , deg	104.4322(1)	93.943(2)
Volume, Å <sup>3</sup>	4774.17(11)	752.07(4)
$Z, Z'$	12, 6	2, 1/2
$T, \text{K}$	173(2)	223(2)
$D_x, \text{g cm}^{-3}$ (@223 K)	1.018	1.061
$\mu(\text{MoK}\alpha)$ , $\text{cm}^{-1}$	0.56	0.59
rflns (collected, indpdnt)	13 786, 9887	2565, 1470
rflns (obs. $2\sigma$ )	5820	1120
$R(F)$ , $R(wF^2)$ , %	13.68, 36.85	5.82, 12.56
Data/parameter	10.2	17.9

$$^a R(F) = \frac{\sum \|F_o\| - |F_c|}{\sum \|F_o\|}; \quad R(wF^2) = \frac{\{\sum [w(F_o^2 - F_c^2)^2]\}}{\sum [w(F_o^2)^2]}^{1/2}; \\ w^{-1} = \sigma^2(F_o^2) + (aP)^2 + bP; \quad P = [2F_c^2 + \max(F_o^2, 0)]/3.$$

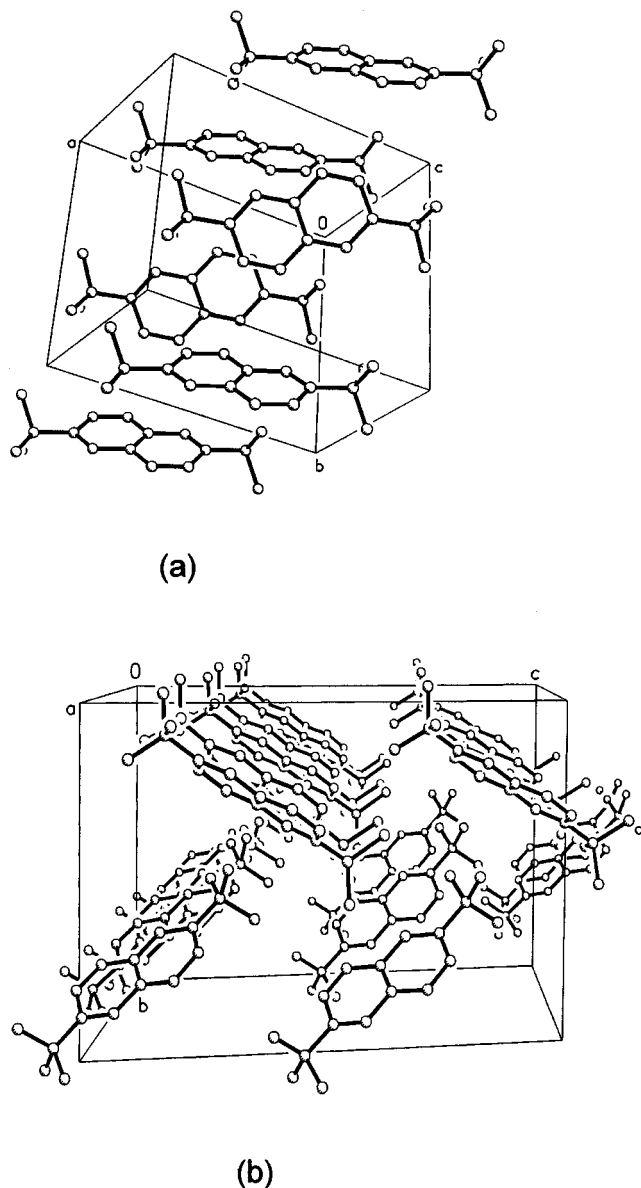


FIG. 2. Unit cell of (a) polymorph **A**, and (b) polymorph **E** of 2,6-DTN. In **A** there are two ( $Z=2$ ) and in **E** there are 12 ( $Z=12$ ) molecules per unit cell. The crystallographically inequivalent molecules are shown in Fig. 3.

gen atoms. There are many possible consequences to the presence of multiple independent molecules in an asymmetric unit. They depend on the spatial relationships among the independent molecules. At one extreme, where there is an absence of correlating spatial relationships, the challenges to the crystallographer are no more difficult than when dealing with a single molecule of comparable size. At the other extreme (represented by **E**), where the lattice positions of the independent molecules differ only very slightly or are simply modulated about a small torsional angle, questions arise concerning the dimensions of the true unit cell. In such cases, the nearly equivalent positions of the independent molecules cause the reflections deriving from the pseudotranslations to dominate, and those from the true lattice (the superlattice) to be systematically much weaker.

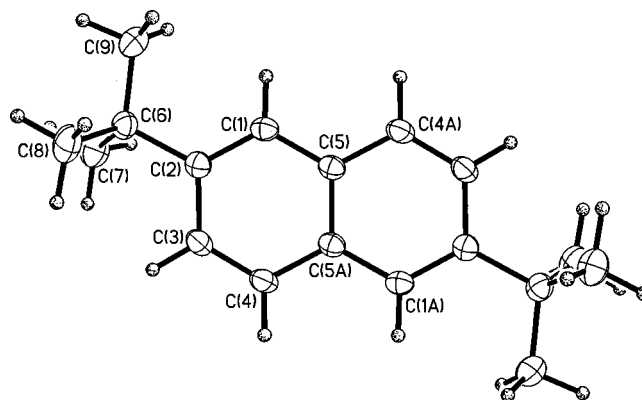


FIG. 3. Crystallographically distinct molecule of 2,6-DTN in **A**. The x-ray diffraction labeling scheme is shown for the unique molecule in **A**. This scheme is different from the organic labeling scheme shown in Fig. 1. The C(5)–C(5a) vector lies in a reflection plane, with the result that there are four crystallographically equivalent half molecules ( $Z'=1/2$ ) in the unit cell.

#### D. Spin-lattice relaxation

Temperature-dependent proton spin-lattice relaxation rates,  $R_1$  ( $=1/T_1$ , where  $T_1$  is the NMR spin-lattice relaxation time) were measured using fixed-frequency Spin-Lock model CPS-2 solid-state NMR spectrometers at Larmor frequencies of 8.50 and 22.5 MHz with a standard inversion-recovery pulse sequence. The relaxation delay was greater than  $8T_1$ . In all cases, the spin-lattice relaxation is exponential, giving a single relaxation rate,  $R_1$ , at each temperature. The typical uncertainty in  $R_1$  is 5%–10%, consistent with the scatter in the data. A calibrated copper–constantan thermocouple was used to monitor sample temperature during the relaxation measurements and the temperature was controlled to at least  $\pm 1$  K. The temperature-dependent  $^1\text{H}$  spin-lattice relaxation rates for the two polymorphs of 2,6-DTN are displayed as logarithmic functions of inverse temperature at two frequencies in Fig. 5. The dynamic state of molecules in **A**, as measured by  $R_1$ , is dramatically different from that of the molecules in **E**.

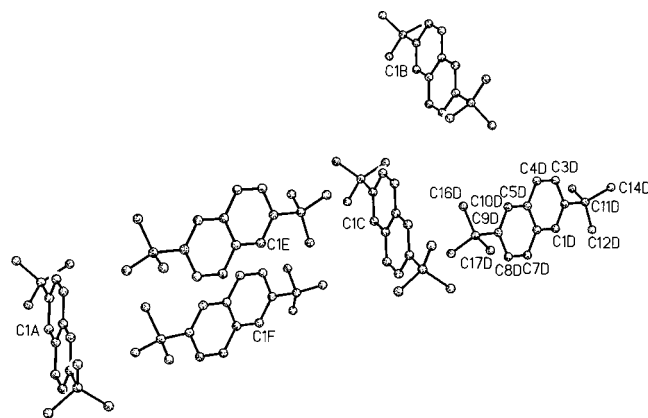


FIG. 4. Crystallographically distinct molecules of 2,6-DTN in **E**. The six crystallographically inequivalent molecules ( $Z'=6$ ) are shown for **E**.

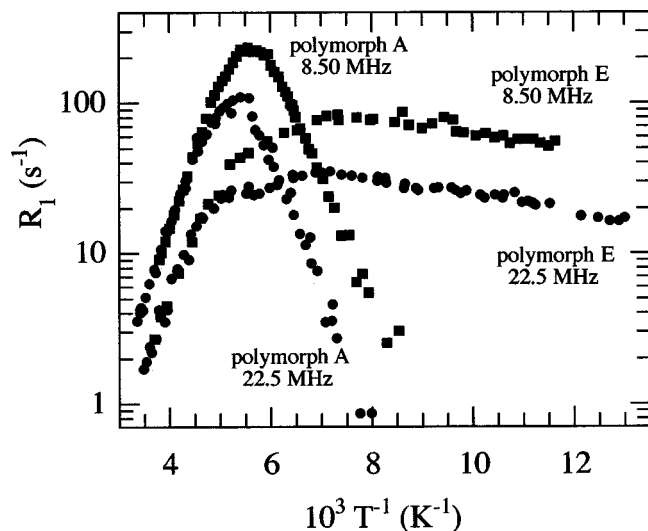


FIG. 5. Proton spin-lattice relaxation rate,  $R_1$ , for A and E (as indicated) as a function of inverse temperature,  $T^{-1}$ .

### E. $^{13}\text{C}$ MAS and solution NMR

$^{13}\text{C}$  CP-MAS NMR spectra ( $t_{CP} = 8$  ms) were obtained at 25.0 MHz with a Chemagnetics m100S spectrometer, and at 75.0 MHz with a Bruker MSL-300 spectrometer. All data were obtained at  $298 \pm 3$  K. The  $^{13}\text{C}$  MAS-NMR spectra of the two polymorphs are shown in Fig. 6, along with a spectrum of 2,6-DTN in  $\text{CDCl}_3$  solution obtained at 100 MHz on a Bruker DRX-400 spectrometer. The spectra of both polymorphs did not depend on field. All resonances of 2,6-DTN are resolved in these spectra and can be assigned, as given in Table II. One does not detect multiple resonances for carbon atoms in crystallographically inequivalent molecules in E.

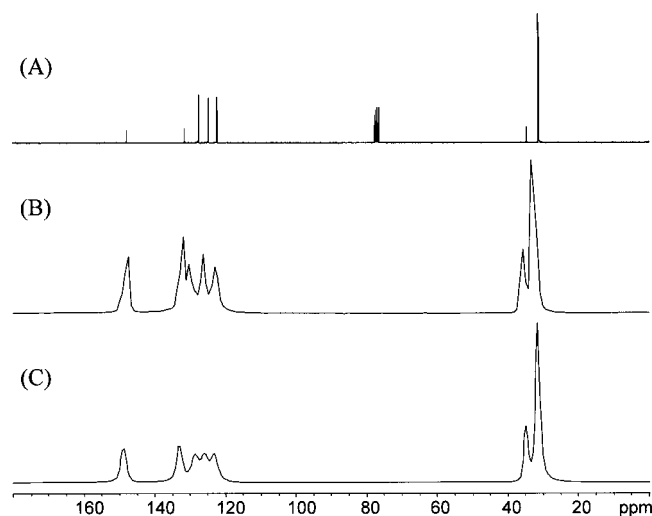


FIG. 6.  $^{13}\text{C}$  NMR spectra of 2,6-DTN: (A) In  $\text{DCl}_3$  solution at 100 MHz; (B) polymorph A at 25 MHz; (C) polymorph E at 25 MHz. Spectra obtained at 75 MHz gave equivalent results to those at 25 MHz. The chemical shifts are given in Table II. The triplet at 77 ppm is the resonance of the carbons in  $\text{DCCl}_3$ , the solvent.

TABLE II.  $^{13}\text{C}$  chemical shifts of the two polymorphs.<sup>a</sup>

Carbon	Solution ppm	Polymorph A ppm	Polymorph E ppm	(A-E) ppm
1, 5	124.7	125.7	125.7	0.0
2, 6	147.9	147.4	149.0	-1.6
3, 7	122.9	122.1	122.9	-0.8
4, 8	127.5	129.8	128.4	1.4
9,10	131.5	131.9	133.2	-1.3
11	31.3	32.6	31.4	1.3
12	34.7	35.5	34.7	1.0

<sup>a</sup>Carbon numbers refer to the numbering in Fig. 1.

## III. DISCUSSION

### A. Zeeman relaxation theory for the protons of 2,6-DTN

For the protons of 2,6-DTN, the random modulation of dipolar interactions between spins by the thermally activated hopping motion is the principal mechanism of relaxation. In solids such as 2,6-DTN, methyl-group and *tert*-butyl-group reorientation is the only motion on the NMR time scale ( $2\pi/\omega_0 \approx 10^{-6}$  s). All other motions in the molecule, such as intramolecular vibration, occur on far too fast a time scale. The relaxation rate  $R_1$  is given by<sup>3</sup>

$$R_1 = \sum_k A_k [j(\omega_0, \tau_k) + 4j(2\omega_0, \tau_k)], \quad (1)$$

where  $j(\omega, \tau)$  is the spectral density and the  $A_k$  are amplitudes that depend on the number and types of motion. The Larmor frequency is  $\omega_0 = \gamma B_0$ , where  $\gamma$  is the proton gyromagnetic ratio and  $B_0$  is the magnetic field strength. The two terms represent, respectively, the effects of single and double spin flips. The number of terms in the sum over  $k$  depends on the number of rotors and the number of motions that modulate the dipolar couplings. The  $A_k$ 's depend on interproton spacings as  $r^{-6}$  and on which spin interactions are modulated. All spin-spin dipolar interactions, whether modulated or not, produce rapid spin diffusion to allow all protons in the sample to relax with a common rate.

The methyl and *tert*-butyl groups reorient subject to a local anisotropic rotational barrier  $V$ . At the temperatures of interest,  $80 < T < 300$  K, the thermal energy,  $kT$ , is much less than  $V$  (where  $k$  is Boltzmann's constant), and the motion may be treated as a random, thermally activated hopping of groups between energetically equivalent orientations. This hopping motion is describable by Poisson statistics.<sup>4</sup> For a rotor characterized by a single mean time,  $\tau$ , between hops, the correlation function is exponential<sup>5</sup>

$$g(t, \tau) = \exp\left(-\frac{|t|}{\tau}\right), \quad (2)$$

where  $\tau^{-1}$  is the mean hop rate. The power spectrum, or spectral density (on which the relaxation rate depends), is the Fourier transform of  $g(t, \tau)$

$$j(\omega, \tau) = \frac{2\tau}{1 + \omega^2 \tau^2}. \quad (3)$$

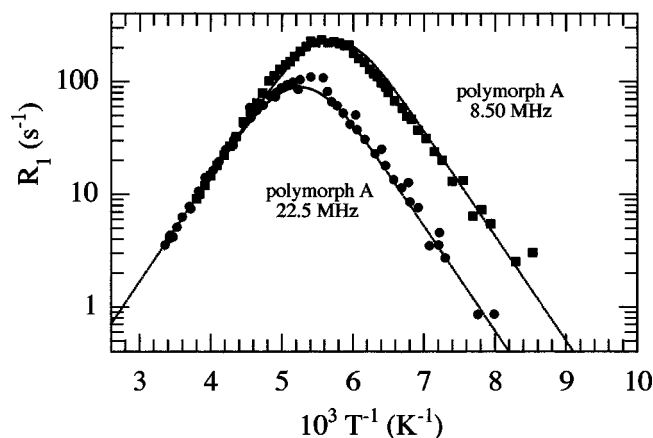


FIG. 7. Fit of the proton spin-lattice relaxation rate,  $R_1$ , versus inverse temperature,  $T^{-1}$ , for A, assuming a single-Poisson process discussed in the text. The data are the same as shown in Fig. 5.

The mean hop rate is determined by the barrier  $V$  through an Arrhenius relationship

$$\tau^{-1} = \tau_{\infty}^{-1} \exp\left(-\frac{V}{kT}\right), \quad (4)$$

where  $\tau_{\infty}^{-1}$  is often interpreted as an attempt frequency to overcome the barrier.<sup>6</sup>

For convenience, experimentally determined values of  $\tau_{\infty}$  are compared with a theoretical value,  $\tilde{\tau}_{\infty}$ , obtained by assuming the rotors undergo harmonic oscillations in the well of a barrier  $V \gg kT$ <sup>6</sup>

$$\tilde{\tau}_{\infty} = \left(\frac{2\pi}{3}\right) \left(\frac{2I}{V}\right)^{1/2}, \quad (5)$$

where  $I$  is the moment of inertia. Using the moment of inertia for a methyl group,<sup>7</sup> it follows that  $\tilde{\tau}_{\infty} = \{(5.34 \times 10^{-13} \text{ s}(\text{kJ mol}^{-1})^{1/2})/V^{1/2}\}$ . This model works surprisingly well for many systems because of the insensitivity of  $\tau_{\infty}$  to the details of the angular dependence of  $V$ .<sup>8</sup>

The temperature dependence of  $R_1$  for A (Figs. 5 and 7) shows there is a unique correlation time for the intramolecular motion inducing proton relaxation in this material. The only motion model consistent with these observed temperature and frequency dependencies is methyl-group reorientation superimposed on *tert*-butyl-group reorientation, with both groups reorienting with the same mean time,  $\tau$ , between hops. The effects of both *tert*-butyl and methyl reorientation may be included as two terms in Eq. (1). The first, characterized by a coefficient  $A_1$ , involves  $\tau$  for the three methyl groups and for the *tert*-butyl group as a whole. The second, characterized by a coefficient  $A_2$ , involves  $\tau/2$  and corresponds to the superimposed motion of methyl and *tert*-butyl reorientation.  $R_1$  is given by<sup>3</sup>

$$R_1 = A_1 [j(\omega_0, \tau) + 4j(2\omega_0, \tau)] + A_2 [j(\omega_0, \tau/2) + 4j(2\omega_0, \tau/2)]. \quad (6)$$

The parameters  $A_1$  and  $A_2$  can be expressed as

$$A_k = \sum_j C_{kj} \left(\frac{\mu_0}{4\pi}\right)^2 \frac{\gamma^4 \hbar^2}{r_{kj}^6}, \quad (7)$$

where the sum is over the various spin-spin interactions. The  $C_{kj}$  are numerical factors of order unity,  $\mu_0$  is the permeability of free space, and the  $r_{kj}$  are various distances found in methyl and *tert*-butyl groups.<sup>3</sup> Under the condition that the intramethyl spin-spin interactions are included in the calculation exactly, but the extra-methyl, intra-*t*-butyl spin-spin interactions are approximated,  $A_1 = A_2 = A_t$ . This equality is a coincidence. The theoretically calculated value of this parameter is given by<sup>3</sup>

$$\tilde{A}_t = \frac{n_t}{N} (2.41 \times 10^{10} \text{ s}^{-2}), \quad (8)$$

where  $n_t$  ( $= 2$  for 2,6-DTN) is the number of *t*-butyl groups in the molecule. For 2,6-DTN,  $\tilde{A}_t = 2.01 \times 10^9 \text{ s}^{-2}$ . When *tert*-butyl-extra-*tert*-butyl proton spin-proton spin interactions are taken into account, an extrapolation of the method of Palmer<sup>9</sup> for *tert*-butylbenzene suggests that  $A_t$  should be 5%–10% larger. Inclusion of intermolecular interactions would make  $A_t$  even larger, perhaps by a few percent.

For a single Poisson process, three independent parameters model the observed nuclear spin-lattice relaxation rate  $R_1$ :  $A_t$ ,  $V$ , and  $\tau_{\infty}$ . As stated above, acceptable values of  $A_t$  and  $\tau_{\infty}$  (called  $\tilde{A}_t$  and  $\tilde{\tau}_{\infty}$ ) fall in certain ranges. Additionally,  $V$  is generally in the range of 5 to 20  $\text{kJ mol}^{-1}$ .<sup>10</sup> The hallmark of a single-Poisson model is that the magnitudes of the slopes  $\partial \ln R_1 / \partial T^{-1}$  at low and high temperature are the same.

## B. Polymorph A

In Fig. 7,  $\ln R_1$  vs  $T^{-1}$  for A is fitted to a single-Poisson process. The model fits the data very well. This result is consistent with the existence of a unique environment for the *tert*-butyl groups indicated by the x-ray diffraction results for this polymorph. The fit at one frequency uniquely determines the fit at the other frequency with no adjustable parameters or, equivalently, the two curves are uniquely determined by a single set of three parameters. From this fit, we conclude that the three methyl groups reorient at the same rate as the *tert*-butyl group. The three fitted parameters are  $V = 18 \pm 3 \text{ kJ mol}^{-1}$ ,  $A_t = (2.6 \pm 0.5) \times 10^9 \text{ s}^{-2}$  [ $A_t/\tilde{A}_t = (1.3 \pm 0.3)$ ], and  $\tau_{\infty} = (6 \pm 2) \times 10^{-14} \text{ s}$  [ $\tau_{\infty}/\tilde{\tau}_{\infty} = (0.5 \pm 0.2)$ ].

As a check on this analysis, we consider another model, in which a single process—methyl-group hopping—modulates the spin interactions. If the *tert*-butyl groups were locked with only methyl-group rotation occurring,  $V$  should be in the range of 9 to 14  $\text{kJ mol}^{-1}$  and the ratio  $A_m/\tilde{A}_m$  (the subscript  $m$  indicates methyl-only rotation) would be approximately 2.6, since  $\tilde{A}_m$  is about half  $\tilde{A}_t$ . This value rules out a methyl-rotation-only model. The fact that additional interactions might contribute to  $\tilde{A}_t$  reasonably suggests that it might be slightly larger than the theoretical value by up to about 30%. This is consistent with the observed  $A_t = (1.3 \pm 0.3)\tilde{A}_t$ . However, it is not reasonable that there are sufficient neglected interactions to increase the value of  $A_m$  by a factor of 2.6.<sup>3</sup>

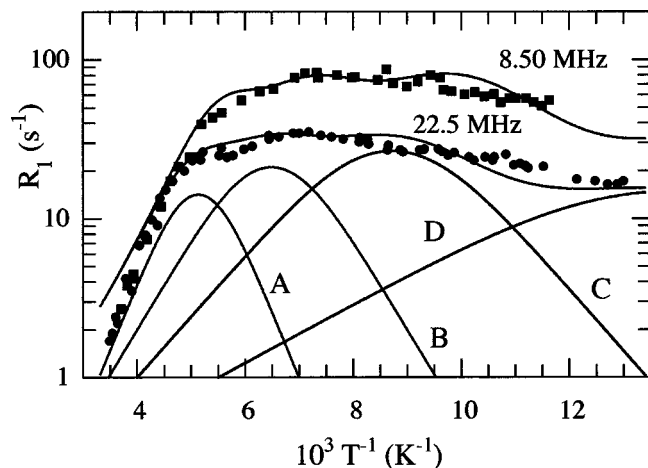


FIG. 8. Proton spin-lattice relaxation rate  $R_1$  versus inverse temperature  $T^{-1}$  for **E** fitted to the sum of four-Poisson processes. The data are the same as in Fig. 5. Lines A, B, C, and D show the theoretical dependencies of the four-Poisson processes at 22.5 MHz. The sum of the four processes is shown. Only the sum at 8.50 MHz is shown.

### C. Polymorph E

The temperature and Larmor frequency dependence of the proton spin-lattice relaxation rate in **A** is a textbook case of the effects of intramolecular reorientation on NMR relaxation rates. The simplest possible model, that of a unique *tert*-butyl environment with random hopping describable by Poisson statistics, fits quantitatively with reasonable values of the fitting parameters. By contrast, the relaxation of protons in **E** is significantly more complex (Fig. 5). To obtain information through analysis of the data, one may assume a model of  $p$  distinct values of  $V$  (due to  $p$  distinct sites). The relaxation rate in this model contains a sum of  $p$  terms, each like Eq. (6), and each with a set of parameters  $\{A_{tk}, \tau_{\infty k}, V_{kj}, k=1, \dots, p$ . An examination of the data for **E** shows that more than four (and probably several more than four) such Poisson processes are required to fit the dependence of  $R_1$  on  $T$  adequately.

As expected, fitting the relaxation data of **E** is more complex than **A**, and a unique fit cannot be obtained. There are simply too many parameters. From the x-ray data, one should assume 12 distinct *tert*-butyl sites, each with a potentially different dynamical environment. However, they are not so different from each other, as seen in the x-ray results and  $^{13}\text{C}$  NMR data, which indicates that the average local environment does not vary greatly when one compares either the two polymorphs or the many independent environments of **E**. In contrast, the relaxation rate is very much more sensitive to the position dependence of the atom-atom potentials.

We first assume a finite number of Poisson processes. (We note that this procedure was carried out before the x-ray data were known.) As an example, the solid lines labeled A, B, C, and D in Fig. 8 show four theoretical relaxation curves at 22.5 MHz for each of four processes. The sum is also shown, with the parameters that describe each process given in Table III. This fit is only intended to serve as an example and a fit to these four processes is, most certainly, not

TABLE III. Parameters for the four-Poisson fit of the temperature dependence of relaxation in polymorph **E**.

Curve	$V$ $\text{kJ mol}^{-1}$	$A_i$ $10^8 \text{ s}^{-2}$	$A_i/\bar{A}_i$	$\tau_{\text{DC}}$ ps	$\tau_{\text{DC}}/\bar{\tau}_{\text{DC}}$
A	16	3.7	0.18	0.32	2.4
B	10	5.5	0.27	1.3	8.1
C	7.3	6.9	0.34	2.8	14
D	3.5	3.8	0.19	17	59

unique. Only the sum is shown for 8.50 MHz. The fit reproduces the general features of the data, but two serious problems arise. First, the discrepancy at the highest temperatures (more than a factor of 2) cannot be rectified by any four-Poisson fit. Second, the range of activation energies (Table III) is far too great; it is not consistent with the crystal structure. Both these problems would doubtless be rectified by a 12-Poisson fit. In particular, the low- $V$  curves C and D are, most likely, sums of several higher  $V$  processes. We note, however, that the four values of  $A_i/\bar{A}_i$  in Table III add to unity, indicating that we properly account for all molecules.

A concern one has with such fitting procedures is the relatively large number of adjustable parameters, 12 for the set in Fig. 8, and the arbitrariness of choosing a model (a sum of four processes) for the motion. Adding more processes (and therefore more adjustable parameters) would obviously lead to a better fit of the data. The x-ray data suggest that fitting these data with up to 12 Poisson processes would be justified, with 25 adjustable parameters (12 values of  $\tau_{\infty}$ , 12 values of  $V$ , and one common value of  $A_i$ ). No doubt a very good fit would result! We consider, though, an alternative fit with fewer parameters.

Another model for the dynamics in **E** is a *continuous* distribution of Poisson processes.<sup>11</sup> For a general process, one describes the system by a continuous distribution,  $\Lambda(\xi)$ , of mean times between hops,  $\xi$ , to give the correlation function

$$g(t) = \int_0^{\infty} \Lambda(\xi) \left[ \exp\left(-\frac{|t|}{\xi}\right) \right] d\xi. \quad (9)$$

The spectral densities are found by Fourier transformation to be

$$j(\omega) = \int_0^{\infty} \Lambda(\xi) \left[ \frac{2\xi}{1 + \omega^2 \xi^2} \right] d\xi, \quad (10)$$

where the distribution function must be normalized

$$\int \Lambda(\xi) d\xi = 1. \quad (11)$$

To obtain further information, one must specify the distribution function. An algebraically tractable  $\Lambda(\xi)$  that has *only one additional parameter* over the single-Poisson model is the Davidson-Cole (DC) model, with a distribution of (Poisson) mean times,  $\xi$ , between hops<sup>11,12</sup>

$$\begin{aligned} \Lambda_{\text{DC}}(\xi, \tau_{\text{DC}}, \varepsilon) &= \frac{\sin(\varepsilon \pi)}{\pi} \frac{1}{\xi} \left( \frac{\xi}{\tau_{\text{DC}} - \xi} \right)^{\varepsilon} & \xi < \tau_{\text{DC}}, \\ &= 0 & \xi > \tau_{\text{DC}}, \end{aligned} \quad (12)$$

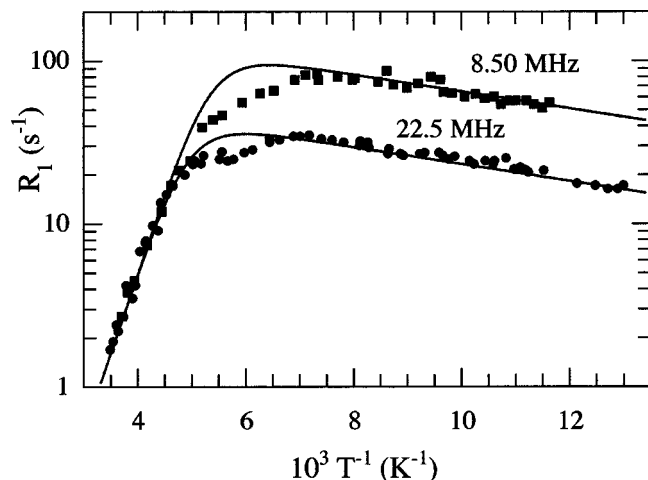


FIG. 9. Proton spin-lattice relaxation rate  $R_1$  versus inverse temperature  $T^{-1}$  for **E** fitted to a single Davidson–Cole distribution as discussed in the text. The data are the same as in Fig. 5.

with

$$\tau_{\text{DC}} = \tau_{\text{DC}\infty} \exp\left(\frac{V_{\text{DC}}}{kT}\right) \quad (13)$$

being an upper cutoff of the distribution of mean hop times.  $V_{\text{DC}}$  is the corresponding cutoff barrier. The parameter  $\varepsilon$  is a measure of the distribution's width. For this distribution, the spectral density has the form<sup>11</sup>

$$j_{\text{DC}}(\omega, \tau_{\text{DC}}, \varepsilon) = \frac{2}{\omega} \frac{\sin[\varepsilon \arctan(\omega \tau_{\text{DC}})]}{(1 + \omega^2 \tau_{\text{DC}}^2)^{\varepsilon/2}}. \quad (14)$$

$R_1$  is then given by Eq. (6), with Eqs. (14) and (13) specifying the spectral density. Practically,  $\varepsilon$  is determined from the ratio of the magnitudes of the low- and high-temperature slopes of  $\ln R$  versus  $T^{-1}$ .<sup>13</sup> In addition, the ratio  $R_1(\omega_a)/R_1(\omega_b) = (\omega_b/\omega_a)^{(1+\varepsilon)}$  at low temperature ( $\omega_a \tau_{\text{DC}}, \omega_b \tau_{\text{DC}} \gg 1$ ) specifies  $\varepsilon$  independently of the high-

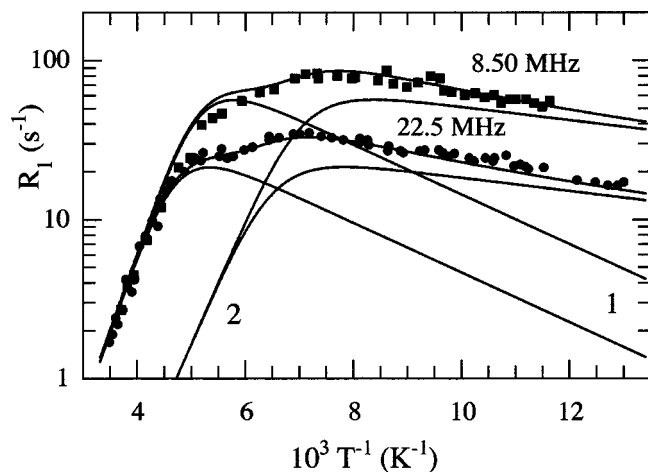


FIG. 10. Proton spin-lattice relaxation rate,  $R_1$ , in **E** versus inverse temperature,  $T^{-1}$ . The pair of solid lines labeled 1 shows the predictions of a single Davidson–Cole process at 8.50 and 22.5 MHz. The pair of solid lines labeled 2 is a second Davidson–Cole curve determined from the difference between the experimental data and the first process. The sum of these two processes is also indicated at the two frequencies.

TABLE IV. Parameters for the fit of the relaxation data for polymorph **E** to a sum of two Davidson–Cole processes.

Curve	$V$ kJ mol <sup>-1</sup>	$\varepsilon$	$A_t$ 10 <sup>9</sup> s <sup>-2</sup>	$A_t/\tilde{A}_t$	$\tau_{\text{DC}}$ ps	$\tau_{\text{DC}}/\tilde{\tau}_{\text{DC}}$
1	19	0.16	1.5	0.75	0.12	1.7
2	15	0.054	3.6	1.8	0.14	0.53

temperature data.<sup>11,13</sup> Thus, measurements at two frequencies overdetermine the fit. Figure 9 shows a fit to a single Davidson–Cole continuous-distribution model. The slope of the plot at high temperatures gives  $V_{\text{DC}} = 18.6 \pm 0.5$  kJ mol<sup>-1</sup>. This value for **E** is the same as the unique  $V$  found for **A** (as can be seen by inspection of Fig. 5), where the relaxation has been seen to be associated with a single-Poisson process. From a weighted average of the slope of the data at low temperature at the two frequencies (since the accuracy is better at 22.5 MHz),  $\varepsilon V_{\text{DC}} = 1.00 \pm 0.04$  kJ mol<sup>-1</sup>, giving a value of  $\varepsilon$  of  $0.054 \pm 0.004$ . These two parameters, although labeled  $V_{\text{DC}}$  and  $\varepsilon$  for the Davidson–Cole fit, characterize the data in a general way. The former characterizes the high-temperature slope and the latter characterizes the ratio of the magnitudes of the low- and high-temperature slopes.

The low- and high-temperature intercepts of the plot are complicated functions of  $A_t$ ,  $\tau_{\text{DC}\infty}$  and  $\varepsilon$  for a Davidson–Cole spectral density.<sup>13</sup> An analysis gives  $A_t = (6.1 \pm 0.9) \times 10^9$  s<sup>-2</sup> and  $\tau_{\text{DC}\infty} = (1.3 \pm 0.4) \times 10^{-13}$  s. These values give  $A_t/\tilde{A}_t = 3.0 \pm 0.5$  and  $\tau_{\text{DC}\infty}/\tilde{\tau}_{\text{DC}\infty} = 1.1 \pm 0.4$ .

These fits successfully characterize some aspects of the unusual relaxation rate behavior, although there are obvious discrepancies outside the experimental error in the vicinity of the maximum of  $R_1$ . In addition, the value of  $A_t/\tilde{A}_t$  is unacceptably large. This alone rules out the model. One may try a slightly more complex fit suggested by the hint of two peaks in the plot of  $R_1$  versus  $T^{-1}$  at 22.5 MHz. Figure 10 shows a fit of the data to a sum of two Davidson–Cole processes, involving the eight parameters given in Table IV. These fits follow the experimental data more closely. One may be tempted to ascribe more significance to the fits than is justified. It is not possible to say that a sum of two Davidson–Cole processes uniquely fits the data. The data were fit sequentially. Curve 1 (shown at both frequencies) represents preliminary fitting of the high-temperature 22.5 MHz data. This determines  $V_{\text{DC}}$  for curve 1. Subsequently,  $A_t$  for the second curve was systematically decreased from a large value, with adjustment of  $\varepsilon$  until the residual between the calculated curve 1 and the experimental data at 22.5 MHz was well-fitted by another single Davidson–Cole fit (curve 2). The two curves and the sum at 8.50 MHz were then uniquely determined with no further adjustable parameters. Although such a procedure may not yield a unique fit, fitting the experimental data at two frequencies restricts quite extensively the acceptable values of parameters. All parameters obtained with the double Davidson–Cole fit have reasonable values. For curve 1,  $V_{\text{DC}}$  is the same as for the fit to a single process,  $19 \pm 1$  kJ mol<sup>-1</sup>. All other parameters have very significantly larger uncertainties than that determined for the

single Davidson–Cole fit, but their values are reasonable.

The fit of the dynamic data with only two distributions suggests that, at least to a first approximation, the 12 *tert*-butyl sites divide into two groups dynamically. Although the parameters of the fit suggest that there may be about twice as many rotors in one group as in the other, we caution that this may be an artifact of the fitting.

#### IV. CONCLUSIONS

2,6-di-*tert*-butylnaphthalene crystallizes in two distinct polymorphic forms. The two polymorphs are similar in most respects, but differ in the number of crystallographically independent *tert*-butyl-group environments. As expected for a rigid molecule, the molecular structure (bond lengths, bond angles) is shown by x ray to be the same within experimental uncertainties in the two forms. Slight differences in the intermolecular arrangement of the molecules change the space group from  $P2_1/c$  for the **A** polymorph ( $Z=2$ ) to  $P2_1$  ( $Z=12$ ) for **E**.  $^{13}\text{C}$  MAS-NMR spectroscopy corroborates that the structure of **A** and **E** are different, but does not find unique signatures for 12 different *tert*-butyl-group environments for **E**. The temperature- and frequency-dependent proton spin-lattice relaxation rates are extremely sensitive to the differences between the two polymorphs. For **A**, the relaxation curves are readily fitted to a model of a single-Poisson process, consistent with the unique *tert*-butyl-group environment observed with x-ray diffraction. The dynamics of the *tert*-butyl-groups in polymorph **E** are observed to be quite different from those of **A**. These require that the dynamics be modeled as a more complex process. This observation is also consistent with the x-ray data, which show 12 unique environments for the *tert*-butyl groups.

The consistency and complementarity of the information from the three techniques served as a guide to analysis. Without the careful structural information of x-ray analysis, the analysis of the relaxation data for **E** would have been an exercise in parametrization of a complex function. On the other hand, the very different dynamics in these two polymorphs seen by relaxation measurements serve to corroborate

the x-ray diffraction data. The  $^{13}\text{C}$  spectroscopy confirmed that the polymorphs were different, but that multiple molecular structures were not involved, in agreement with x-ray results.

#### A. Supplementary material available

CIF files containing details of the crystallographic work are available from one of the authors (A.L.R.) and have been deposited in the Cambridge Crystallographic Database in conjunction with Ref. 1.

#### ACKNOWLEDGMENTS

C.D. acknowledges support of the Petroleum Research Fund of the American Chemical Society [Grant #33633] during the course of some of this work.

- <sup>1</sup>A preliminary communication of this work has been published. A. L. Rheingold, J. S. Figueroa, C. Dybowski, and P. A. Beckmann, *Chem. Commun.* (Cambridge) 651 (2000).
- <sup>2</sup>H. M. Crawford and M. C. Glesmann, *J. Am. Chem. Soc.* **76**, 1108 (1954).
- <sup>3</sup>P. A. Beckmann, A. I. Hill, E. B. Kohler, and H. Yu, *Phys. Rev. B* **38**, 11098 (1988).
- <sup>4</sup>S. Clough, *Physica* (Utrecht) **136**, 145 (1986).
- <sup>5</sup>N. G. Van Kampen, *Stochastic Processes in Physics and Chemistry* (North-Holland, Amsterdam, 1981).
- <sup>6</sup>N. L. Owen, in *Internal Rotations in Molecules*, edited by W. J. Orville-Thomas (Wiley, New York, 1974), p. 157.
- <sup>7</sup>W. H. Flygare, *Molecular Structure and Dynamics* (Prentice-Hall, Englewood Cliffs, NJ, 1978).
- <sup>8</sup>S. Clough and A. Heidemann, *J. Phys. C* **13**, 3585 (1980).
- <sup>9</sup>C. A. Palmer, Ph.D. dissertation, Bryn Mawr College, 1991.
- <sup>10</sup>P. A. Beckmann, H. A. Al-Hallaq, A. M. Fry, A. L. Plofker, B. A. Roe and J. A. Weiss, *J. Chem. Phys.* **100**, 752 (1994); P. A. Beckmann, in *Physics and Chemistry of Finite Systems: From Clusters to Crystals*, edited by P. Jena, S. N. Khanna, and B. K. Rao (Kluwer Academic, Amsterdam, 1992), Vol. 1, p. 357; A. M. Fry, P. A. Beckmann, A. J. Fry, P. C. Fox, and A. Isenstadt, *J. Chem. Phys.* **95**, 4778 (1991); P. A. Beckmann, *Phys. Rev. B* **39**, 12248 (1989).
- <sup>11</sup>P. A. Beckmann, *Phys. Rep.* **171**, 85 (1988).
- <sup>12</sup>D. W. Davidson and R. H. Cole, *J. Chem. Phys.* **19**, 1484 (1951).
- <sup>13</sup>K. G. Conn, P. A. Beckmann, C. W. Mallory, and F. B. Mallory, *J. Chem. Phys.* **87**, 20 (1987).